Available at www.sciencedirect.com

ScienceDirect

journal homepage: www.elsevier.com/locate/he

# Rare earth oxide modified $CuO/CeO_2$ catalysts for the water–gas shift reaction

Yusheng She [a], Qi Zheng [a,*], Lei Li [b], Yingying Zhan [a], Chongqi Chen [a], Yuanhui Zheng [c], Xingyi Lin [a]

[a] National Engineering Research Center of Chemical Fertilizer Catalysts, Fuzhou University, Gongye Road 523, Fuzhou, Fujian 350002, PR China
[b] College of Biological and Chemical Engineering, Jiaxing University, Jiaxing, Zhejiang 314001, PR China
[c] Materials Engineering, Monash University, Clayton, VIC 3800, Australia

ARTICLE INFO

*Article history:*
Received 21 July 2009
Received in revised form
27 August 2009
Accepted 28 August 2009
Available online 19 September 2009

*Keywords:*
$CuO/CeO_2$ catalyst
Doped
WGSR
Rare earth oxide
Selective $N_2O$ chemisorption

ABSTRACT

Water–gas shift reaction was carried out over a series of $CuO/CeO_2$ catalysts doped with trivalent rare earth oxide ($RE_2O_3$, RE = Y, La, Nd and Sm), prepared via co-precipitation method. The effect of the dopants on the structure and catalytic properties of $CuO/CeO_2$ catalysts was investigated with the aid of X-ray diffraction (XRD), Raman spectra, $N_2$ physisorption, $H_2$-TPR and selective $N_2O$ chemisorption characterizations. The results reveal the beneficial role of $La_2O_3$ and $Nd_2O_3$ doping in increasing the WGS catalytic activities and stabilities of $CuO/CeO_2$ catalysts, while the addition of $Y_2O_3$ and $Sm_2O_3$ leads to the negative effect. Correlating to the characteristic results, it is found that the performance of $CuO/CeO_2$–$RE_2O_3$ catalysts strongly depends on their surface copper dispersion, microstrain value and the amount of oxygen vacancies generated in ceria lattice. Besides, enough evidences suggest that, the most effective active site for WGS reaction is the moderate copper oxide (crystalline) interacted with surface oxygen vacancies of ceria in the CuO–$CeO_2$ system.



## 1. Introduction

Hydrogen is a potential solution for satisfying many of our energy needs against the environment pollution while reducing carbon dioxide and other greenhouse gas emissions. At present, nearly 95% of the hydrogen supply is produced from the reforming of crude oil, coal, natural gas, biomass and so on [1,2]. However, the reformed fuel contains 1–10% CO, which degrades the performance of the Pt electrode in fuel cell system [3,4]. To get clean hydrogen for fuel cells and other industrial applications, the water–gas shift (WGS) reaction and CO oxidation processes are critical. To accelerate them, heterogeneous catalysts are frequently used [5]. Copper oxide catalysts supported on ceria, are gaining popularity for various reactions, among them very important one is the WGS reaction [6,7]. As reported in previous studies [8–10], $CuO/CeO_2$ catalyst exhibits excellent WGS reactivity comparable to those of commercial precious metal catalysts. Moreover, Cu and Ce abundance, as well as lower costs compared to precious metals, make them strongly competitive.

Oxygen storage capacity (OSC), strong metal-support interactions (SMSI) and rich oxygen vacancies in the ceria-based catalysts are generally believed to have a pronounced positive effect on catalytic performance toward WGS reaction and other catalytic applications [10–12]. In this sense, metal-doped ceria has been the subject of considerable interest for

* *Corresponding author*. Tel.: +86 591 8373 1234 8112; fax: +86 591 8373 8808.
E-mail address: qizheng2005@gmail.com (Q. Zheng).
0360-3199/$ – see front matter © 2009 Professor T. Nejat Veziroglu. Published by Elsevier Ltd. All rights reserved.
doi:10.1016/j.ijhydene.2009.08.062

a long time in view of their higher oxygen storage capacity and better reducibility than pure ceria [13]; besides, the addition of different metal dopants with valences lower than (4+) to $CeO_2$ can increase the concentration of oxygen vacancies and improve the thermal stability of parent oxide [14–16]. Although WGS reaction has been studied extensively, there are only several papers on WGS activity of doped-ceria catalysts [5,17–22]. Li et al. have studied that La-doped-ceria retained a small crystallite size (7 nm) and medium high surface area after calcination at 650 °C [5]. Fraga et al. have revealed that dispersion of vanadia onto $Pt/CeO_2$ increase the catalytic activity up to a vanadium surface density of 6 V atoms/$nm^2$ [17]. Fraga et al. have also found that the presence of magnesium improved ceria reduction favoring the creation of OH groups, which are considered the key factor for the WGS reaction [18]. Wang and Gorte have demonstrated that the WGS activity of Pd/ceria catalysts can be enhanced by the addition of monolayer coverage of $Fe_2O_3$ on ceria, while the addition of monolayer coverages of Tb, Gd, Y, Sn, Sm, Pr, Eu, Bi, Cr, and V to ceria had minimal effect on the reaction rates [19]. Likewise, few papers investigating the metal oxides modified $CuO/CeO_2$ catalysts can be found either. Papavasiliou et al. have reported on the effect of type and content of eight different dopant cations on the catalytic properties of $CuO–CeO_2$ system in the reaction of methanol steam reforming [23]. In our group's previous study, we have shown that the addition of $Al^{3+}$ to $CuO–CeO_2$ system has a positive effect on the WGS activity as well as the stability of CuO and ceria against agglomeration [24].

The dopant cations with ionic radius and electronegativity close to those of cerium cation are thought to be the most appropriate modifiers of structural and chemical properties of ceria [25]. The similarity of the ionic radii is also the criterion to predict the presence or not of significant solid solubility. In this connection, the rare earth elements could be a good choice. In fact, the rare earth elements, with paramagnetism and other excellent properties, have been widely used in the form of oxides into catalyst formulations as structural or electronic promoters to improve the activity, selectivity and thermal stability of the catalysts [26,27].

In the present study, a series of $CuO/CeO_2$ catalysts doped with trivalent rare earth oxides ($RE_2O_3$, RE = Y, La, Nd and Sm) were synthesized by co-precipitation method. The influence of the dopants on the structural, redox properties and, as a consequence, the WGSR catalytic activity of $CuO/CeO_2$ catalysts was investigated in detail. The results reveal that improved WGS catalytic activity and thermal stability of $CuO/CeO_2$ catalyst could be achieved by the modification of certain rare earth oxide, correlating well with the information from the X-ray diffraction (XRD), Raman spectra, $N_2$ physisorption, selective $N_2O$ chemisorption and $H_2$-TPR characterizations.

## 2. Experimental

### 2.1. Catalysts preparation

Doped copper–cerium mixed oxide catalysts were prepared via parallel co-precipitation method. Nitrate salts of copper [$Cu(NO_3)_2 \cdot 3H_2O$], cerium [$Ce(NO_3)_3 \cdot 6H_2O$] and rare-earth modifier [$RE(NO_3)_3 \cdot nH_2O$ (RE = Y, La, Nd and Sm) ] were dissolved in deionized water with fixed copper content (25 wt. %, calculated as CuO) and modifier content (5 wt. %, calculated as $RE_2O_3$). Then the mixed aqueous solution were co-precipitated with an aqueous solution of KOH under vigorous stirring at T = 80 °C and pH = 10 ± 1. A black suspension was acquired and then aged with continuous stirring at 80 °C for 6 h. The resulting precipitate was centrifuged and washed by deionized water for several times, then dried at 120 °C for 12 h and finally calcined at 650 °C for 4 h (heating rate: 5 °C/min) in air.

### 2.2. Characterizations

The crystalline structure of the as-synthesized samples was analyzed by means of X-ray powder diffractometer (PANalytical X' pert Pro) operated at 40 kV and 40 mA employing Co-Kα radiation (λ = 0.17902 nm). The crystal size of ceria and copper oxide was determined from the peak broadening with the Scherrer equation. The BET surface area and pore volume were measured on a Micromeritics ASAP 2020 physical adsorption analyzer, at −196 C using nitrogen as adsorbate. Prior to each analysis, the sample was degassed at 200 °C for 3 h to obtain a residual pressure of less than $10^{-5}$ Torr. Cu-dispersion was determined by selective $N_2O$ chemisorption method at 50 C with 3.3 vol%$N_2O$/He mixed gas stream on pretreated (He), completely reduced (10%$H_2$/Ar) and degassed (He) CuO/doped-$CeO_2$ catalyst samples. The mass of every sample equals to 50 mg and the flowing rate of $N_2O$/He gas steam was set at 20 mL/min. A freeze trap submerged in liquid nitrogen was employed to remove all traces of $N_2O$ from the residual mixed gas after the reaction ($N_2O + 2Cu = Cu_2O + N_2$). The resultant nitrogen was detected by the TCD connected to an AutoChem 2910 apparatus. The surface copper dispersion of the catalysts was defined as the molar ratio of surface Cu to total Cu loaded. Both test temperature (50 °C) and flowing rate of $N_2O$/He gas steam (20 mL/min) were meticulously chosen in order to minimize in-depth Cu and $CeO_2$-x oxidation, thus obtaining reliable Cu-dispersion values [28]. Raman spectra were collected at room temperature on a Renishaw Invia Plus system. The samples were excited with a 514.5 nm laser line. Temperature-programmed reduction (TPR) measurement was carried out on an AutoChem 2910 instrument. The $H_2$-TPR was performed by passing 10% $H_2$/Ar (flowing rate = 30 mL/min) on 50 mg catalyst at a heating rate of 10 C/min. Prior to TPR, the samples were pretreated under Argon atmosphere at 200 °C for 30 min. Then the system was cooled to ambient temperature under a pure Argon gas. The hydrogen consumption was monitored using a thermal conductivity detector (TCD).

### 2.3. Evaluation of catalytic performance

The catalytic activities and thermal stabilities of the catalysts for WGS reaction were tested in a fixed bed reactor at atmospheric pressure. 2 g of catalysts (30–40 mesh) was placed between two layers of quartz granules inside a stainless steel tube (i.d. = 12 mm). The reaction temperature was monitored by a pair of thermocouples, which are inserted into the center of the catalyst bed and fixed by the reactor wall, respectively. The experiment was directly performed under a feed gas (10% CO, 60% $H_2$, 12% $CO_2$ and balance $N_2$) flowing at 103.7 mL/min

without pre-reduction. The ratio of vapor to feed gas was maintained at 1:1. The residual water of the outlet was removed by a condenser before entering a gas chromatograph (102 G) equipped with a thermal conductivity detector (TCD). The activity was expressed by the conversion of CO, defined as: $X_{CO}$ (%) = (1–$V'_{CO}/V_{CO}$)×100%/(1+$V'_{CO}$), where $V_{CO}$ and $V'_{CO}$ are the inlet and outlet content of CO, respectively. The catalytic activity was first measured from 200 to 400 °C, then kept at 400 °C for 10 h and decreased to 200 °C. The second evaluating cycle was run from 200 to 400 °C again to investigate the thermal stability of the catalysts.

## 3. Results and discussion

### 3.1. *Structural studies of the as-prepared CuO/$CeO_2$ catalysts*

The XRD patterns of CuO/$CeO_2$–$RE_2O_3$ catalysts, as well as that of non-modified CuO/$CeO_2$ sample, are presented in Fig. 1. The strong diffraction peaks of $CeO_2$ and CuO are detected in all the samples: those marked with "◆" are indexed to cubic fluorite $CeO_2$ (JCPDS file no.34–0394), while the others marked with "#" are indexed to monoclinic CuO (JCPDS file no.05–0661). To further investigate the effect of doping on the structure of CuO/$CeO_2$ catalysts, some micro-structure parameters (e.g., crystal size, the cell parameter and micro-strain value) were calculated from the XRD results by Rietveld analysis. The results are shown in Table 1.

The results of average crystal size of $CeO_2$ reveal that all the additives inhibit the crystal growth of ceria and favor the formation of smaller particles, except for $Sm_2O_3$, which causes nearly no change in crystal size. The most obvious lessening is caused by modification of $La_2O_3$. Contrarily, it can also

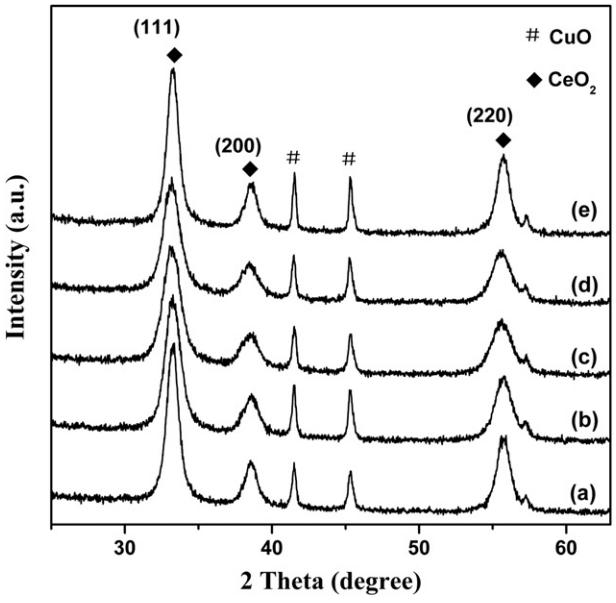


**Fig. 1 – XRD patterns of the CuO/$CeO_2$–$RE_2O_3$ catalysts: (a) CuO/$CeO_2$, (b) CuO/$CeO_2$–$Y_2O_3$, (c) CuO/$CeO_2$–$La_2O_3$, (d) CuO/$CeO_2$–$Nd_2O_3$, (e) CuO/$CeO_2$–$Sm_2O_3$.**

be observed that the average crystallite size of CuO increases in all cases with the addition of dopants.

No obvious diffraction lines, ascribed to dopants or their derivates, are detected, which suggests that the dopants might enter the $CeO_2$ frame and form an oxide solid solution with ceria. As we know, the tetravalent cations, such as $Ce^{4+}$, have an eight-coordination of oxygen ions. The unit cell contains four cations occupying the opposite four corners. These tetravalent cations can be replaced by trivalent (e.g. $Y^{3+}$, $La^{3+}$, $Nd^{3+}$, $Sm^{3+}$) or divalent cations (e.g. $Cu^{2+}$). Synchronously, oxygen vacancies are generated by this substitution and are desirable in redox-type reactions [29]. From Fig. 1, it should be noted that doping causes a slight shift of ceria peaks in some cases, which is indicative for the dissolution of the dopants in the cubic fluorite lattice. Another evidence for the formation of solid solution is the variation of lattice constant "a" for ceria, as shown in Table 1. The lattice constant of the cubic cell of ceria in CuO/$CeO_2$ catalyst was found to be equal to 0.5412 nm, in agreement with previous studies [23,30]. When the CuO/$CeO_2$ catalysts were doped with rare earth oxides, the lattice constant increases and XRD reflections of the doped ceria are shifted to lower degrees. It should be ascribed to their incorporation into ceria lattice and their higher ionic radii than that of $Ce^{4+}$ (e.g. $La^{3+}$ (0.116 nm)>$Ce^{4+}$ (0.097 nm)).

Compared to non-modified CuO/$CeO_2$ catalyst, it can be found that with the addition of rare earth oxide, there is a distinct increase in the microstrain values, except for the case of $Sm_2O_3$, and the largest value is obtained for the one doped with $La_2O_3$ (0.577 for $CeO_2$ and 0.232 for CuO). Such strong microstrain increment estimated for these samples suggests that copper has also been incorporated into the ceria fluorite lattice effectively upon the modified CuO/$CeO_2$ catalyst, which might occur at the interface between CuO and $CeO_2$ [31,32], thus enhancing the synergistic interaction between them.

The structural studies of the as-synthesized CuO/$CeO_2$–$RE_2O_3$ catalysts are also complemented by Raman characterization presented in Fig. 2. One can see that the Raman spectra show a strong main line at about 440 $cm^{-1}$ for all samples, which corresponds to the triply degenerate $F_{2g}$ mode and can be viewed as a symmetric breathing mode of the oxygen atoms around Ce ions [33]. A weak Raman band at around 1160 $cm^{-1}$, relating to the presence of $CeO_2$ defect [34], can also be observed in all cases. Another broad weak band occurs at about 580 $cm^{-1}$, which has been attributed to oxygen vacancies created in the ceria structure [35]. As labeled in Fig. 2, it shows increasing relative intensity following such a sequence: (c) > (d) > (a) > (e) > (b), indicating that the amount of oxygen vacancies of the as-synthesized catalysts can be ranked as: CuO/$CeO_2$–$La_2O_3$ > CuO/$CeO_2$–$Nd_2O_3$ > CuO/$CeO_2$ > CuO/$CeO_2$–$Sm_2O_3$ > CuO/$CeO_2$–$Y_2O_3$. In addition, the full width at the half of maximum (FWHM) of the main line was calculated and the results are inserted in Fig. 2. It is found that the addition of the studied dopants influences the FWHM value of main line in different ways. The presence of $La_2O_3$ and $Nd_2O_3$ leads to an increase of FWHM value (39.8 → 46.9 and 40.2 $cm^{-1}$), while in the case of $Sm_2O_3$ and $Y_2O_3$, the effect is opposite (39.8 → 32.3 and 39.4 $cm^{-1}$). It is generally agreed that the FWHM value of main ceria line depends strongly on

**Table 1 – Microstructure results and texture properties of the as-synthesized catalysts.**

| Sample | CuO content (wt.%)[a] | Cell parameter (nm) | Crystal size (nm) | | Microstrain (Δd/d) (%) | | $S_{BET}$ ($m^2$/g) | | Pore volume (mL/g) |
|---|---|---|---|---|---|---|---|---|---|
| | | a ($CeO_2$) | $CeO_2$ | CuO | $CeO_2$ | CuO | Fresh | Used[b] | |
| $CuO/CeO_2$ | 22.9 | 0.5412 | 11.5 | 43.7 | 0.291 | 0.169 | 42 | 33 | 0.25 |
| $CuO/CeO_2$–$Y_2O_3$ | 22.2 | 0.5414 | 8.9 | 53.9 | 0.407 | 0.167 | 39 | 20 | 0.24 |
| $CuO/CeO_2$–$La_2O_3$ | 22.0 | 0.5432 | 8.0 | 50.1 | 0.577 | 0.232 | 53 | 44 | 0.38 |
| $CuO/CeO_2$–$Nd_2O_3$ | 21.9 | 0.5431 | 8.3 | 50.8 | 0.483 | 0.214 | 51 | 35 | 0.32 |
| $CuO/CeO_2$–$Sm_2O_3$ | 22.1 | 0.5416 | 11.8 | 74.0 | 0.256 | 0.146 | 32 | 27 | 0.21 |

a The actual CuO content was analyzed by atomic absorption spectrometry (AAS).
b The catalysts undergone the activities and thermal stabilities test and were cooled to ambient temperature without feed gas.

ceria dispersion as well as on the defects in ceria lattice, including oxygen vacancies [36,37]. Since the average size of ceria does not differ very much for the samples, the widening is more likely to be connected to the formation of oxygen vacancies in ceria. So it is confirmed that the formation of oxygen vacancies is facilitated by the doping of $La_2O_3$ and $Nd_2O_3$ whereas weakened in case of $Sm_2O_3$ and $Y_2O_3$. In addition, it's known that the structure of the fluorite assembly tolerates a high level of atomic disorder upon the incorporation of metal cations into ceria, and the crystal lattice must compensate for the excess negative charge by three mechanisms: vacancy compensation, cerium interstitial compensation and dopant interstitial compensation. For small cations the vacancy compensation is mostly accompanied by some compensation via dopant interstitial, while in the case of dopants with large radius, the vacancy compensation is the preferred route [38]. So in our study, the oxygen vacancies can be generated by the incorporation of dopant cations (with large ionic radii) and $Cu^{2+}$ into ceria lattice for charge balance, in good agreement with the results of XRD characterization.

Furthermore, one can see that, for the $F_{2g}$ mode, the Raman bands of catalysts shift to lower wavenumber when the rare earth oxides are added (except for $Sm_2O_3$). The shift of Raman bands should be related to changes of $CeO_2$ environment with the addition of rare earth oxide as dopants, which affects the polarizability of the symmetrical stretching mode of [Ce-$O_8$] vibrational unit. McBride et al. [35] have also reported such systematic shift to lower frequency when studying $Ce_{1-x}RE_xO_{2-y}$ (RE = La, Pr, Nd, Eu, Gd, Tb). The occurrence of Raman bands' shift is consistent with the increase of microstrain values from XRD results, both of which probably originate from the influence of synergistic interaction between CuO species and ceria support. Combining the results from the Raman spectra and XRD characterization above, it is indicated that a certain amount of copper ions as well as the $RE^{3+}$ dopants have been incorporated into ceria lattice along with the formation of oxygen vacancies for charge balance, thus effectively enhancing the synergistic interaction between CuO species and ceria support.

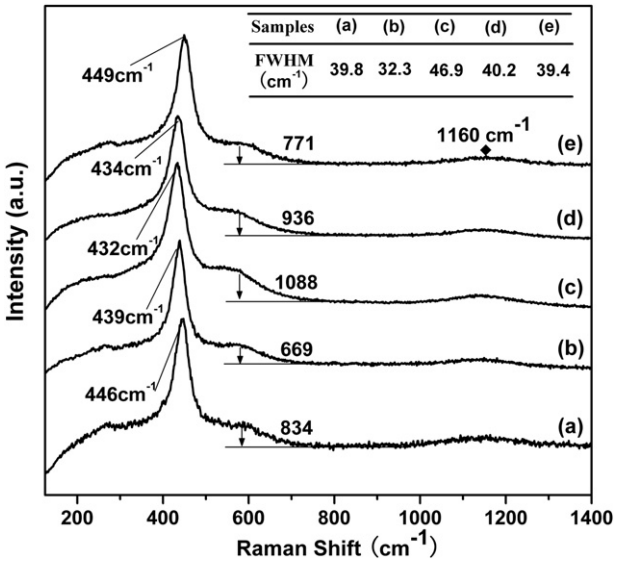


**Fig. 2 – Raman spectra of $CuO/CeO_2$–$RE_2O_3$ catalysts excited by 514.5 nm laser line: (a) $CuO/CeO_2$, (b) $CuO/CeO_2$–$Y_2O_3$, (c) $CuO/CeO_2$–$La_2O_3$, (d) $CuO/CeO_2$–$Nd_2O_3$, (e) $CuO/CeO_2$–$Sm_2O_3$.**

### 3.2. *Texture and copper dispersion of as-prepared $CuO/CeO_2$ catalysts*

The specific surface area ($S_{BET}$) and pore volume of the as-synthesized $CuO/CeO_2$ and $CuO/CeO_2$–$RE_2O_3$ catalysts are also reported in Table 1. As presented in Table 1, modification by $La_2O_3$ and $Nd_2O_3$ leads to increase of $S_{BET}$, while addition of $Y_2O_3$ and $Sm_2O_3$ cause the opposite effect. The change in total pore volume of as-synthesized catalysts follows the same trend. Significant increase of pore volume is observed after doping with $La_2O_3$. The surface area of used catalysts is smaller than that of the fresh ones in all cases (e.g., decreased by 48.7% for $CuO/CeO_2$–$Y_2O_3$), which may be attributed to the agglomeration of supports or collapse of pores occurring during the WGS activity evaluation.

It is reported that [28], nitrous oxide can be used for the estimation of the surface area of metallic copper in copper-based catalysts, since $N_2O$ oxidizes the surface atoms of Cu-crystals selectively in a temperature interval from 20 to 120 °C by the reaction: $N_2O + 2Cu = Cu_2O + N_2$. From the consumption of $N_2O$ or the evolvement of $N_2$ one can calculate the copper dispersion directly according to the stoichiometry of the above Equation. Besides, from knowledge of the area taken up by a copper surface atom, the surface area of copper can also be assessed.

Fig. 3 shows the nitrogen signal from the TCD as a function of the time elapsed after switching the valve that admits $N_2O$ into the feed stream. The curves consist of two overlapping

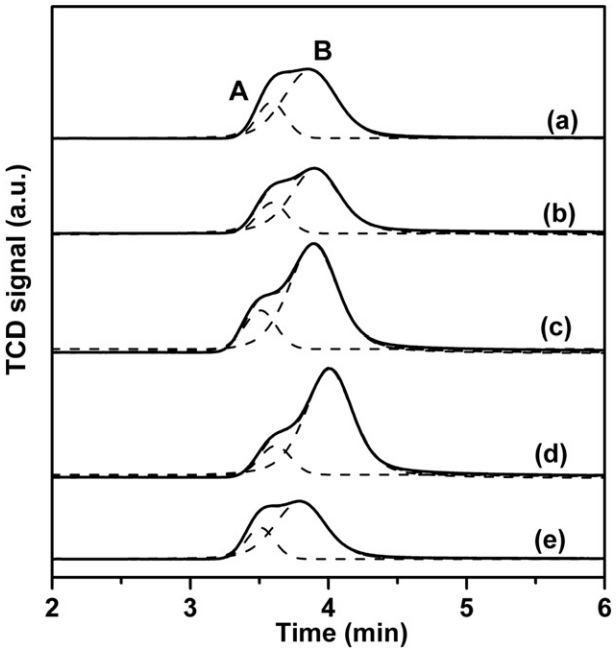


**Fig. 3 – The TCD-signal for nitrogen as a function of time over various samples: (a) $CuO/CeO_2$, (b) $CuO/CeO_2$–$Y_2O_3$, (c) $CuO/CeO_2$–$La_2O_3$, (d) $CuO/CeO_2$–$Nd_2O_3$, (e) $CuO/CeO_2$–$Sm_2O_3$. All measurements were carried out under the same procedure.**

peaks for all samples, which have been fitted by Gauss-Lorentz method as dotting lines in. It can be observed that, in all cases, the area of peak B is larger than that of peak A. In addition, considering that the exterior copper (on the surface of ceria) is easier to be oxided by $N_2O$ compared to the interior one (on the wall of the pore channels), the peaks A and B might be ascribed to the amount of $N_2$ engendered by the exterior and interior Cu, respectively. Further calculated results based on the complete integral value of curves (e.g. the total amount of nitrogen evolved in the measurement) are listed in Table 2. The Cu-dispersion values are 10%, 9.9%, 16.2%, 14.2% and 8.1% for the $CuO/CeO_2$, $CuO/CeO_2$–$Y_2O_3$, $CuO/CeO_2$–$La_2O_3$, $CuO/CeO_2$–$Nd_2O_3$ and $CuO/CeO_2$–$Sm_2O_3$ samples, respectively. Besides, the specific metallic copper surface area of samples was also assessed providing that the reduced copper surface has a density of $1.46 \times 10^{19}$ Cu atoms/$m^2$, as reported in the literature [39]. It should be noted that the trend of copper dispersion, as well as the specific metallic copper surface area, is well consistent with that of $S_{BET}$ values of as-synthesized catalysts. Therein, the presence of $La_2O_3$ and $Nd_2O_3$ as modifier increases the well-dispersed copper species over the ceria support, which is generally believed to be one of the positive factors for high WGS reactivity [9,40].

### 3.3. *Redox properties of as-prepared $CuO/CeO_2$ catalysts*

Fig. 4 shows the $H_2$-TPR profiles of doped $CuO/CeO_2$ catalysts. The profile of non-modified $CuO/CeO_2$ catalyst is also included for comparison purposes. Each curve in Fig. 4 exhibits three reduction peaks, i.e. a low temperature peak at about 140 °C, denoted as peak α, and two overlapping peaks at about 175 °C and 200 °C, denoted as peak β and γ, respectively. In our previous study, the assignment of these peaks had been studied concretely by means of treating the catalysts with $(NH_4)_2CO_3$ solution [41]. It's demonstrated that peak α and β should be ascribed to the reduction of non-crystalline copper oxide in close contact with ceria and moderate copper oxide (crystalline) interacted with surface oxygen vacancies of ceria, respectively. As for peak γ, it has been attributed to the reduction of small part of surface ceria, the copper oxide incorporated into the ceria lattice and the large isolated copper oxide phase (crystalline), which does not associate with $CeO_2$.

From Fig. 4, one can see the addition of $La_2O_3$ and $Nd_2O_3$ shifts significantly all reductive peaks to lower temperatures compared to the non-modified $CuO/CeO_2$ catalyst. However, in the case of $Y_2O_3$ and $Sm_2O_3$ containing samples, all the peaks are slightly shifted to higher temperatures. These results reveal that doping with $La_2O_3$ and $Nd_2O_3$ can enhance the reducibility of $CuO/CeO_2$ catalysts, while the $Y_2O_3$ and $Sm_2O_3$ containing samples become less reducible. Interestingly, it can be found that the area of peak β for these samples follows the same trend, with the highest one being the $CuO/CeO_2$–$La_2O_3$ sample, which indicates that the La-doped catalyst possesses higher amount of moderate copper oxide species interacted with surface oxygen vacancies of ceria than the other samples. And at this point, the sample $CuO/CeO_2$–$Nd_2O_3$ locates in the following place. Moreover, it should be

**Table 2 – Copper-dispersion and copper surface area estimated at a $N_2O$-titration temperature of 50 °C for $CuO/CeO_2$–$RE_2O_3$ catalysts.**

| Sample | Cu-dispersion[a] (%) | Copper surface atoms (μmol/g cat) | Specific copper surface area[b] ($m^2$/g cat) |
|---|---|---|---|
| $CuO/CeO_2$ | **10.0** (1.5, 8.5) | 320 | 13.2 |
| $CuO/CeO_2$–$Y_2O_3$ | **9.9** (1.2, 8.7) | 317 | 13.1 |
| $CuO/CeO_2$–$La_2O_3$ | **16.2** (1.9, 14.3) | 518 | 21.4 |
| $CuO/CeO_2$–$Nd_2O_3$ | **14.2** (1.9, 14.0) | 454 | 18.7 |
| $CuO/CeO_2$–$Sm_2O_3$ | **8.1** (1.2, 6.9) | 259 | 10.7 |

The total Cu content is 3.2 mmol/g cat (20% w/w).
a The values in parentheses show the contributions of peak A and B, respectively.
b In the calculation of the copper surface area, it is assumed that the reduced copper surface has a density of $1.46 \times 10^{19}$ Cu atoms/$m^2$ [27], NA = $6.02 \times 10^{23}$/mol.

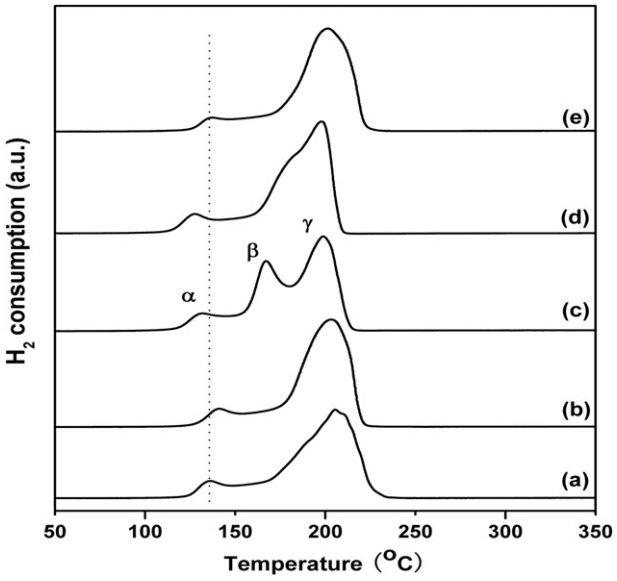


**Fig. 4 – $H_2$-TPR profiles of the $CuO/CeO_2$–$RE_2O_3$ catalysts: (a) $CuO/CeO_2$, (b) $CuO/CeO_2$–$Y_2O_3$, (c) $CuO/CeO_2$–$La_2O_3$, (d) $CuO/CeO_2$–$Nd_2O_3$, (e) $CuO/CeO_2$–$Sm_2O_3$.**

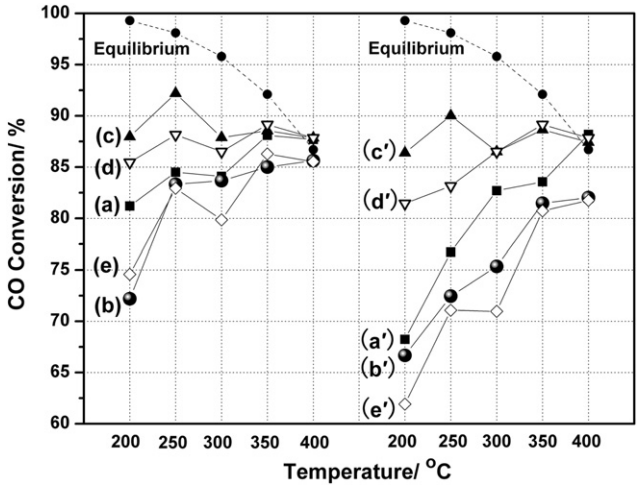


**Fig. 5 – Performance of WGS reaction over $RE_2O_3$ doped $CuO/CeO_2$ catalysts. Feed gas: 10% CO, 60% $H_2$, 12% $CO_2$ and balance $N_2$; Vapor–gas: 1:1 (mol); $W/F = 1.54\ g\ s\ cm^{-3}$. After the first cycle, the catalysts were successively exposed to the feed gas at the given temperature procedure (keep at 400 °C for 10 h and then cool to 200 °C), and then start the second evaluation cycle. The first cycle: (a) $CuO/CeO_2$ (b) $CuO/CeO_2$–$Y_2O_3$, (c) $CuO/CeO_2$–$La_2O_3$, (d) $CuO/CeO_2$–$Nd_2O_3$, (e) $CuO/CeO_2$–$Sm_2O_3$; the second cycle: (a′) $CuO/CeO_2$, (b′) $CuO/CeO_2$–$Y_2O_3$, (c′) $CuO/CeO_2$–$La_2O_3$, (d′) $CuO/CeO_2$–$Nd_2O_3$, (e′) $CuO/CeO_2$–$Sm_2O_3$.**

noted that the variation of peak β area is also basically consistent with that of the microstrain values and the amount of oxygen vacancies generated in ceria. Therefore, it is inferred that the interaction between the CuO species and surface oxygen vacancies of ceria can be promoted by the substitutional incorporation of copper ions and modifiers (e.g. $La^{3+}$, $Nd^{3+}$) into ceria lattice along with the increase of oxygen vacancies. This process leads to the distortion of the ceria lattice due to the presence of multiple cation-oxygen distances other than the single cation-oxygen bond distance existing in pure ceria lattice [42], finally resulting in the increase of microstrain values and the evolution of Raman bands.

### 3.4. *Catalytic performance of as-prepared $CuO/CeO_2$ catalysts*

Fig. 5 shows CO conversion curves versus temperature over pure and $RE_2O_3$ doped $CuO/CeO_2$ catalysts. The dopants have different effects on catalytic behavior of the modified $CuO/CeO_2$ catalysts. For the first cycle, it is clear that a positive effect is caused by the addition of La- and Nd- dopants, while the presence of $Y_2O_3$ and $Sm_2O_3$ leads to the opposite effect. The CO conversion of $CuO/CeO_2$-$La_2O_3$ catalyst reaches the maximum with the value of 92.2% at 250 °C, which is an increment of 9.1% compared to that of non-modified $CuO/CeO_2$ catalyst (84.5%) at the same temperature. A comparison between the activities of the as-synthesized samples in the first and second cycle shows that the CO conversions of $CuO/CeO_2$-$Y_2O_3$, $CuO/CeO_2$–$La_2O_3$, $CuO/CeO_2$–$Nd_2O_3$, $CuO/CeO_2$–$Sm_2O_3$ and non-modified $CuO/CeO_2$ catalyst decrease by 8.2%, 1.4%, 4.9%, 2.1% and 19.1% at 200 °C, respectively. Therefore, it can be concluded that the thermal stability of the as-prepared $CuO/CeO_2$ catalysts is improved by the modification of rare earth oxides, especially by the introduction of $La_2O_3$ (only 1.4%). The result of catalytic activity evaluation correlates well with the analysis of XRD, Raman spectra, BET, selective $N_2O$ chemisorption and $H_2$-TPR characterizations.

To begin with, from the structural characterizations, it is found that the variation of catalytic activity is in agreement with that of the microstrain value of as-synthesized catalysts, which were demonstrated by XRD characterizations. The microstrain originates from the interaction between copper oxide and ceria, which presents in the form of the incorporation of copper ions (accompanied by dopant cations) into ceria lattice, as has been reported for other systems [32,43–45]. For the $CuO/CeO_2$ catalysts modified by $La_2O_3$ and $Nd_2O_3$, both the CuO and $CeO_2$ possess higher microstrain, as a consequence, higher surface energy and catalytic activity for WGS reaction. In addition, from the analysis of Raman spectra characterization, there is a noteworthy correlation between the amount of oxygen vacancies created in the ceria structure and the WGS activity of $CuO/CeO_2$ catalysts. The sample with more oxygen vacancies also exhibits higher WGS activity. Hence, it is established that rich oxygen vacancies generated in the ceria structure play a positive role for higher WGS activity because they can increase the diffusion rate of active oxygen in the $CuO/CeO_2$ catalysts.

It should also be pointed out that the variation of WGS activity of as-prepared catalysts presents the same trend as that of their surface copper dispersion, which was assessed by

means of selective $N_2O$ chemisorption characterization. It is generally believed that optimum catalytic properties of CuO/$CeO_2$ catalysts can be achieved in the presence of well-dispersed copper species over ceria support [40]. Accordingly, the $La_2O_3$ and $Nd_2O_3$ modified catalysts, with better Cu-dispersion and larger specific surface area of metallic copper (as presented in Table 2), show better catalytic performance for WGS reaction. By contraries, the poor catalytic performance of CuO/$CeO_2$–$Y_2O_3$ and CuO/$CeO_2$–$Sm_2O_3$ catalysts might be mainly related to their lower $S_{BET}$, total pore volume, and surface copper dispersion.

Form the analysis of redox characterization, conclusion can be easily drawn that, the larger the area of peak β in the $H_2$-TPR profile is, the better WGS activity CuO/$CeO_2$ catalyst will be. The most obvious variation of peak β in TPR profiles happens in the case of La-doped sample, which also exhibits the highest catalytic activity and stability for WGS reaction. On the other hand, the CuO/$CeO_2$ catalysts doped with $Y_2O_3$ and $Sm_2O_3$, which show smaller area of peak β in their TPR profiles, have little WGS activity especially at the temperature of 200 °C. These results reveal that the number of the moderate CuO particles (crystalline) interacted with surface oxygen vacancies of ceria plays a significant role for high activity of CuO/$CeO_2$ catalyst. And it could be suggested that the WGS reaction might take place preferentially on the copper/ceria interface, in more detail, on the Cu-$O_{vacancy}$ interface, which is in agreement with the results of previous studies [41,46]. In addition, the reducibility of doped CuO/$CeO_2$ catalysts also has effect on the catalytic activity in present study. As shown in the TPR profiles, La- and Nd- doped CuO/$CeO_2$ catalysts with higher catalytic activity are more reducible than the other investigated samples, appearing as the shifting of peaks to lower temperature.

## 4. Conclusions

CuO/$CeO_2$ catalysts doped with $RE_2O_3$ (RE = Y, La, Nd and Sm) prepared by co-precipitation were evaluated for WGS reaction in present work. A positive modification has been achieved with $La_2O_3$ and $Nd_2O_3$ as dopants, while the $Y_2O_3$ and $Sm_2O_3$ doped catalysts go to the opposite way. It is found that the better performance of La- and Nd-doped catalysts can be attributed to larger BET surface area and total pore volume, better surface copper dispersion, enhanced reducibility and stronger synergistic interaction between copper oxide and ceria. In addition, according to the result of Raman analysis, it is elucidated that the amount of oxygen vacancies could be facilitated by the incorporation of $La^{3+}$ and $Nd^{3+}$ into the ceria lattice. It is also found that the variation of catalytic activity is in very agreement with that of the area of the reductive peak β in $H_2$-TPR, suggesting that the most effective copper species for WGS reaction is the moderate CuO (crystalline) interacted with surface oxygen vacancies of ceria. Besides, the thermal stability of the as-synthesized CuO/$CeO_2$ catalysts can be improved to some extent by the modification of rare earth oxides, especially, the one doped with $La_2O_3$, showing a potential industrial applicability for the low temperature WGS reaction.

## Acknowledgements

The authors acknowledge the financial support from the Department of Science of the People's Republic of China (20771025) and the Department of Science of Fujian Province (2007J0221).

## REFERENCES

[1] Jacobson MZ, Colella WG, Golden DM. Cleaning the air and improving health with hydrogen fuel-cell vehicles. Science 2005;308:1901–5.
[2] Sirichaiprasert K, Luengnaruemitchai A, Pongstabodee S. Selective oxidation of CO to $CO_2$ over Cu–Ce–Fe–O composite-oxide catalyst in hydrogen feed stream. Int J Hydrogen Energy 2007;32:915–26.
[3] Spivey JJ. Catalysis in the development of clean energy technologies. Catal Today 2005;100(1–2):171–80.
[4] Liu Y, Fu Q, Flytzani-Stephanopoulos M. Preferential oxidation of CO in $H_2$ over CuO–$CeO_2$ catalysts. Catal Today 2004;93–95:241–6.
[5] Li Y, Fu Q, Flytzani-Stephanopoulos M. Low-temperature water–gas shift reaction over Cu- and Ni-loaded cerium oxide catalysts. Appl Catal B: Environ 2000;27:179–91.
[6] Jacobs G, Khalid S, Patterson PM, Sparks DE, Davis BH. Water–gas shift catalysis: kinetic isotope effect identifies surface formates in rate limiting step for Pt/ceria catalysts. Appl Catal A: Gen 2004;268:255–66.
[7] Gunawardana PVDS, Lee HC, Kim DH. Performance of copper-ceria catalysts for water gas shift reaction in medium temperature range. Int J Hydrogen Energy 2009;34:1336–41.
[8] Zimmer P, Tsch öpe A, Birringer R. Temperature-programmed reaction spectroscopy of ceria- and Cu/ceria-supported oxide catalyst. J Catal 2002;205:339–45.
[9] Djinovic P, Batista J, Pinta A. Calcination temperature and CuO loading dependence on CuO–$CeO_2$ catalyst activity for water–gas shift reaction. Appl Catal A: Gen 2008;347:23–33.
[10] Qi XM, Flytzani-Stephanopoulos M. Activity and stability of Cu–$CeO_2$ catalysts in high-temperature water–gas shift for fuel-cell applications. Ind Eng Chem Res 2004;43:3055–62.
[11] Shan WJ, Shen WJ, Li C. Structural characteristics and redox behaviors of $Ce_{1-x}Cu_x$ $O_y$ solid solutions. Chem Mater 2003; 15:4761–7.
[12] Shiau CY, Ma MW, Chuang CS. CO oxidation over $CeO_2$-promoted Cu/γ-$Al_2O_3$ catalyst: effect of preparation method. Appl Catal A: Gen 2006;301:89–95.
[13] Andreeva D, Ivannov I, Ilieva L, Abrashev MA. Gold catalysts supported on ceria and ceria–alumina for water–gas shift reaction. Appl Catal A: Gen 2006;302:127–32.
[14] Palmqvist AEC, Johansson EM, Jaras SG, Muhammed M. Total oxidation of methane over doped nanophase cerium oxides. Catal Lett 1998;56:69–75.
[15] Marino F, Baronetti G, Laborde M, Bion N, Le Valant A, Epron F, et al. Optimized CuO–$CeO_2$ catalysts for COPROX reacion. Int J Hydrogen Energy 2008;33:1345–53.
[16] Zhang Y, Anderson S, Muhammed M. Nanophase catalytic oxides: I. Synthesis of doped cerium oxides as oxygen storage promoters. Appl Catal B: Environ 1995;6:325–37.
[17] Duarte de Farias AM, Bargiela P, Rocha MGC, Fraga MA. Vanadium-promoted Pt/$CeO_2$ catalyst for water–gas shift reaction. J Catal 2008;260:93–102.
[18] Duarte de Farias AM, Barandas APMG, Perez RF, Fraga MA. Water–gas shift reaction over magnesia-modified Pt/$CeO_2$ catalysts. J Power Sources 2007;165:854–60.

[19] Wang X, Gorte RJ. The effect of Fe and other promoters on the activity of Pd/ceria for the water–gas shift reaction. Appl Catal A: Gen 2003;247:157–62.
[20] Fu Q, Kudriavtseva S, Saltsburg H, Flytzani-Stephanopoulos M. Gold–ceria catalysts for low-temperature water–gas shift reaction. Chem Eng J 2003;93:41–53.
[21] Wheeler C, Jhalani A, Klein EJ, Tummala S, Schmidt LD. The water–gas-shift reaction at short contact times. J Catal 2004; 223:191–9.
[22] Panagiotopoulou P, Kondarides D. Effect of the nature of the support on the catalytic performance of noble metal catalysts for the water–gas shift reaction. Catal Today 2006; 112:49–52.
[23] PaPavasiliou J, Avgouropoulos G, Ioannides T. Effect of dopants on the performance of CuO–$CeO_2$ catalysts in methanol steam reforming. Appl Catal B: Environ 2007;69: 226–34.
[24] Li L, Zhan YY, Zheng Q, Zheng YH, Lin XL, Li DL, et al. Water–gas shift reaction over aluminum promoted Cu/CeO2 nanocatalysts characterized by XRD, BET, TPR and Cyclic Voltammetry (CV). Catal Lett 2007;118:91–7.
[25] Etsell TH, Flengas SN. The electrical properties of solid oxide electrolytes. Chem Rev 1970;70:339–76.
[26] Colussi S, Leitenburg CD, Dolcetti G, Trovarelli A. The role of rare earth oxides as promoters and stabilizers in combustion catalysts. J Alloys and Compounds 2004;374:387–92.
[27] Ilieva L, Pantaleo G, Ivanov I, Zanella R, Venezia AM, Andreeva D. A comparative study of differently prepared rare earths-modified ceria-supported gold catalysts for preferential oxidation of CO. Int J Hydrogen Energy 2009;34: 6505–15.
[28] Jensen JR, Johannessen T, Livbjerg H. An improved $N_2O$-method for measuring Cu-dispersion. Appl Catal A: Gen 2004;266:117–22.
[29] Park JW, Jeong JH, Yoon WL, Jung H, Lee HT, Lee DK, et al. Activity and characterization of the Co-promoted CuO–$CeO_2$/$\gamma$-$Al_2O_3$ catalyst for the selective oxidation of CO in excess hydrogen. Appl Catal A: Gen 2004;274: 25–32.
[30] Liu YY, Hayakawa T, Tsunoda T, Suzuki K, Hamakawa S, Murata K, et al. Steam reforming of methanol over Cu/$CeO_2$ catalysts studied in comparison with Cu/ZnO and Cu/Zn(Al)O catalysts. Top Catal 2003;22:205–13.
[31] Zhou XD, Huebner W. Size-induced lattice relaxation in $CeO_2$ nanoparticles. Appl Phys Lett 2001;79:3512–4.
[32] Gamarra D, Munuera G, Hungr ía AB, Fern ández-García M, Conesa JC, Midgley PA, et al. Structure-activity relationship in nanostructured copper-ceria-based preferential CO oxidation catalysts. J Phys Chem C 2007;111: 11026–38.
[33] Lin XM, Li LP, Li GS, Su WH. Transport property and Raman spectra of nanocrystalline solid solutions $Ce_{0.8}Nd_{0.2}O_{2-\delta}$ with different particle size. Mater Chem Phys 2001;69:236–40.
[34] Liu ZG, Zhou RX, Zheng XM. Influence of residual $K^+$ on the catalytic performance of CuO–$CeO_2$ catalysts in preferential oxidation of CO in excess hydrogen. Int J Hydrogen Energy 2008;33:791–6.
[35] McBride JR, Hass KC, Poindexter BD, Weber WH. Raman and X-ray studies of $Ce_{1-x}RE_xO_{2-y}$, where RE = La, Pr, Nd, Eu, Gd and Tb. J Appl Phys 1994;76:2435–41.
[36] Graham GW, Weber WH, Peters CR, Usmen R. Empirical method for determining $CeO_2$-particle size in catalysts by Raman spectroscopy. J Catal 1991;130:310–3.
[37] Kosacki I, Suzuki T, Anderson HU, Colomban P. Raman scattering and lattice defects in nanocrystalline $CeO_2$ thin films. Solid State Ionics 2002;149:99–105.
[38] Trovarelli A. Catalytic properties of ceria and $CeO_2$-containing materials. Catal Rev Sci Eng 1996;38:439–520.
[39] Evans JW, Wainwright MS, Bridgewater AJ, Young DJ. On the determination of copper surface area by reaction with nitrous oxide. Appl Catal 1983;7:75–83.
[40] Chen HL, Zhu HY, Wu Y, Gao F, Dong L, Zhu JJ. Dispersion, reduction and catalytic properties of copper oxide supported on Ce0.5Zr0.5$O_2$ solid solution. J Mol Catal A: Chem 2006;255: 254–9.
[41] Li L, Zhan YY, Zheng Q, Zheng YH, Chen CQ, She YS, et al. Water–gas shift reaction over CuO/$CeO_2$ catalysts: effect of the thermal stability and oxygen vacancies of $CeO_2$ supports prepared by different methods. Catal Lett 2009;130:532–40.
[42] Ketchik SV, Plyasova LM, Seredkin AE, Kostrov VV, Morozov LN. X-ray studies of supported copper–aluminium catalysts. React Kinet Catal Lett 1980;14:429–34.
[43] Si R, Zhang YW, Li SJ, Lin BX, Yan CH. Urea-based hydrothermally derived homogeneous nanostructured $Ce_{1-x}Zr_xO_2$ (x = 0–0.8) solid solutions: a strong correlation between oxygen storage capacity and lattice strain. J Phys Chem B 2004;108:12481–8.
[44] Jiang XY, Lu GL, Zhou RX, Mao JX, Chen Y, Zheng XM. Studies of pore structure, temperature-programmed reduction performance, and micro-structure of CuO/$CeO_2$ catalysts. Appl Surface Sci 2001;173:208–20.
[45] Kasatkin I, Kurr P, Kniep B, Trunschke A, Schlogl R. Role of lattice strain and defects in copper particles on the activity of Cu/ZnO/$Al_2O_3$ catalysts for methanol synthesis. Angew Chem Int Ed 2007;46:7324–7.
[46] Wang XQ, Rodríguez JA, Hanson JC, Gamarra D, Martínez-Arias A, Fern ández-García M. In situ studies of active sites for the water gas shift reaction over Cu–$CeO_2$ catalysts: complex interaction between metallic copper and oxygen vacancies of ceria. J Phys Chem B 2006;110:428–34.